Journal Name

ARTICLE

Spin-crossover compounds based on iron(II) complexes of 2,6-bis(pyrazol-1-yl)pyridine (bpp) functionalized with carboxylic acid and ethyl carboxylic acid

Received 00th January 20xx,
Accepted 00th January 20xx

DOI: 10.1039/x0xx00000x

www.rsc.org/

Víctor García-López,[a] Mario Palacios-Corella,[a] Alexandre Abhervé,[a] Isaac Pellicer-Carreño,[a] Cédric Desplanches,[b] Miguel Clemente-León*[a] and Eugenio Coronado*[a]

Four new salts of the iron(II) complex of 2,6-bis(pyrazol-1-yl)pyridine ligand functionalized with a carboxylic acid group (bppCOOH) of formulas $[Fe(bppCOOH)_2](BF_4)_2$ (**1(BF$_4$)$_2$**), $[Fe(bppCOOH)_2](CF_3SO_3)_2{\cdot}yMe_2CO$ (**1(CF$_3$SO$_3$)$_2$·yMe$_2$CO**), $[Fe(bppCOOH)_2](AsF_6)_2{\cdot}yMe_2CO$ (**1(AsF$_6$)$_2$·yMe$_2$CO**) and $[Fe(bppCOOH)_2](SbF_6)_2{\cdot}yMe_2CO$ (**1(SbF$_6$)$_2$·yMe$_2$CO**) have been prepared and characterized together with a more complete structural and photomagnetic characterization of the previously reported $[Fe(bppCOOH)_2](ClO_4)_2$ (**1(ClO$_4$)$_2$**). Furthermore, the iron(II) complex of the ethyl ester derivative of bppCOOH (bppCOOEt) has been prepared and characterized (compound $[Fe(bppCOOEt)_2](ClO_4)_2{\cdot}yMe_2CO$, **2(ClO$_4$)$_2$·yMe$_2$CO**). Isostructural **1(BF$_4$)$_2$** and **1(ClO$_4$)$_2$** show an abrupt and reversible spin transition with a much lower $T_{1/2}$ for the BF_4^- salt. $CF_3SO_3^-$, SbF_6^- and AsF_6^- counteranions and bppCOOEt ligand lead to the incorporation of solvent molecules in the structures, which play an important role in the spin crossover properties of these compounds. In the case of **1(CF$_3$SO$_3$)$_2$·yMe$_2$CO**, a reversible spin transition is obtained after desolvation. All these compounds show LIESST effect.

Introduction

Spin-crossover (SCO) complexes contain a metal ion which can be reversibly switched between two distinct spin states, low-spin (LS) and high-spin (HS) with a variety of external inputs, such as temperature, light, pressure, magnetic or electric field.[1] SCO compounds have been proposed for many applications, such as sensors, memories or spintronics.[2]

One of the most studied families of SCO compounds are bis-chelated iron(II) complexes of the tridentate ligand 2,6-bis(pyrazol-1-yl)pyridine (bpp) as they usually present very abrupt spin transitions close to room temperature.[3] In addition, they exhibit spin-crossover induced by irradiation: Light-Induced Excited Spin State Trapping effect (LIESST) at relatively high temperatures.[4] Furthermore, they are a versatile family from the chemical point of view as substitution in the pyridine ring allows functional groups to be included at the periphery of the $[Fe(bpp)_2]^{2+}$ centre without perturbing the SCO properties. In a previous work, we prepared the iron(II) complex of bpp ligand functionalized with a carboxylic acid (bppCOOH, see Scheme 1).[5] This resulted in the SCO compound $[Fe(bppCOOH)_2](ClO_4)_2$, which forms an extended 1D network built via hydrogen-bond intermolecular interactions. This leads to an abrupt spin transition with $T_{1/2}$ ($T_{1/2}$ = temperature of 50 % HS⟶LS conversion) of ca. 380 K and a T(LIESST) of 60 K (T(LIESST) is the relaxation temperature of the photoinduced HS state). The presence of a carboxylic acid group in this complex has been used for the preparation of polynuclear metal complexes,[6] and for the anchoring to metal-oxide surfaces,[7] a necessary step for the preparation of many devices. Very recently, it has been shown that Co(II) complexes of bppCOOH and related ligands may exhibit a Single-molecule Magnet behavior.[8,9]

In this work, we have completed the structural and photomagnetic characterization of $[Fe(bppCOOH)_2](ClO_4)_2$ (**1(ClO$_4$)$_2$**) and prepared and characterized new salts of the $[Fe(bppCOOH)_2]^{2+}$ complex with BF_4^-, $CF_3SO_3^-$, SbF_6^- and AsF_6^- counterions. Moreover, we have prepared the iron(II) complex of the ethyl ester derivative of bppCOOH (bppCOOEt, see Scheme 1) in compound $[Fe(bppCOOEt)_2](ClO_4)_2{\cdot}yMe_2CO$ (**2(ClO$_4$)$_2$·yMe$_2$CO**). This has led to a variety of SCO behaviors, which could help to understand the role played by the carboxylic acid group and that of the intermolecular interactions, solvent molecules, and counteranions in the SCO properties of this family of compounds.

[a] Instituto de Ciencia Molecular (ICMol), Universidad de Valencia, C/ Catedrático José Beltrán 2, 46980 Paterna, Spain. Fax: 34 963543273; Tel: 34 963544419; E-mail: miguel.clemente@uv.es.
[b] Université de Bordeaux, ICMCB, 87 avenue du Dr. A. Schweitzer, Pessac, F-33608, France.

† Electronic Supplementary Information (ESI) available: ESI contains structural views, thermal dependence of the unit cell parameters, powder X-ray diffraction patterns, Thermogravimetric analysis, magnetic and photomagnetic properties and crystallographic data of the compounds.

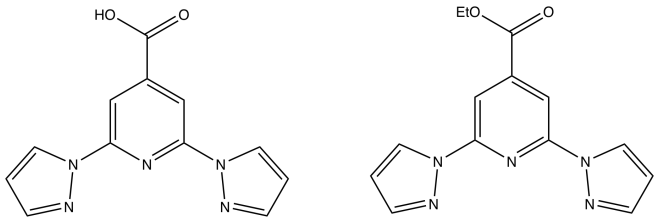

Scheme 1. Molecular structure of bppCOOH (left) and bppCOOEt (right) in compounds $[Fe(bppCOOH)_2](ClO_4)_2$ (**1(ClO$_4$)$_2$**) $[Fe(bppCOOH)_2](BF_4)_2$ (**1(BF$_4$)$_2$**), $[Fe(bppCOOH)_2](CF_3SO_3)_2{\cdot}yMe_2CO$ (**1(CF$_3$SO$_3$)$_2$·yMe$_2$CO**), $[Fe(bppCOOH)_2](AsF_6)_2{\cdot}yMe_2CO$ (**1(AsF$_6$)$_2$·yMe$_2$CO**), $[Fe(bppCOOH)_2](SbF_6)_2{\cdot}yMe_2CO$ (**1(SbF$_6$)$_2$·yMe$_2$CO**) and $[Fe(bppCOOEt)_2](ClO_4)_2{\cdot}yMe_2CO$ (**2(ClO$_4$)$_2$·yMe$_2$CO**).

Results and discussion

Synthesis.

The two ligands were obtained by literature procedures. bppCOOEt was obtained by esterification with ethanol of bppCOOH.[10] $[Fe(bppCOOH)_2](ClO_4)_2$ (**1(ClO$_4$)$_2$**),[5] $[Fe(bppCOOH)_2](BF_4)_2$ (**1(BF$_4$)$_2$**), $[Fe(bppCOOH)_2](CF_3SO_3)_2{\cdot}yMe_2CO$ (**1(CF$_3$SO$_3$)$_2$·yMe$_2$CO**) and $[Fe(bppCOOEt)_2](ClO_4)_2{\cdot}yMe_2CO$ (**2(ClO$_4$)$_2$·yMe$_2$CO**) were obtained by slow diffusion of diethyl ether into solutions of the Fe(II) salts and bppCOOH or bppCOOEt in a 1:2 molar ratio in acetone. $[Fe(bppCOOH)_2](AsF_6)_2{\cdot}yMe_2CO$ (**1(AsF$_6$)$_2$·yMe$_2$CO**) and $[Fe(bppCOOH)_2](SbF_6)_2{\cdot}yMe_2CO$ (**1(SbF$_6$)$_2$·yMe$_2$CO**) were synthesized with the same procedure but the Fe(II) salt was prepared in situ by reacting $FeCl_2$ with $AgAsF_6$ or $AgSbF_6$ in a 1:2 molar ratio. In contrast to $[Fe(bppCOOH)_2]^{2+}$, $[Fe(bppCOOEt)_2]^{2+}$ does not form solvent-free salts. By changing the concentration of the metal and ligand, three different solvates were isolated one containing water molecules ($[Fe(bppCOOEt)_2](ClO_4)_2(H_2O)_3$ and two containing acetone molecules monoclinic $[Fe(bppCOOEt)_2](ClO_4)_2{\cdot}1.5Me_2CO$ and triclinic $[Fe(bppCOOEt)_2](ClO_4)_2{\cdot}yMe_2CO$. The acetone solvates could be separated easily as they present different morphology (needles or prisms). We have focused our studies on the triclinic acetone solvate of formula $[Fe(bppCOOEt)_2](ClO_4)_2{\cdot}yMe_2CO$ (**2(ClO$_4$)$_2$·yMe$_2$CO**) as it was not possible to obtain pure samples of the other solvates. The formation of so many solvates could be related to the flexibility of the ethyl group.

Structure of $[Fe(bppCOOH)_2](ClO_4)_2$ (1(ClO$_4$)$_2$) and $[Fe(bppCOOH)_2](BF_4)_2$ (1(BF$_4$)$_2$).

The structure of **1(ClO$_4$)$_2$** at 120 K was solved by single crystal X-ray diffraction in a previous work.[5] This structure corresponds to the LS state. In this work, we have solved the structure at 400 K, which is very close to the HS state as shown by metal-ligand distances and magnetic properties (see below). Furthermore, we have measured powder X-ray diffraction (PXRD) patterns of powdered crystals of **1(ClO$_4$)$_2$** from 298 to 400 K.

1(ClO$_4$)$_2$ and **1(BF$_4$)$_2$** crystallize in monoclinic crystal system with centrosymmetric *C*2/*c* space group. The asymmetric unit is composed by half $[Fe(bppCOOH)_2]^{2+}$ cation and one perchlorate or tetrafluoroborate anion. The central iron(II) ion of the complex is coordinated by six nitrogen atoms from two tridentate bppCOOH ligands with a distorted octahedral coordination geometry. The Fe-N bond lengths at 120 K (1.888(4)-1.981(2) Å for **1(ClO$_4$)$_2$**[5] and 1.889(3)-1.974(6) Å for **1(BF$_4$)$_2$**) clearly indicate that the complexes are in the LS state, whereas longer Fe-N bond lengths at 400 K for **1(ClO$_4$)$_2$** (2.113(6)-2.159(5) Å) and at 350 K for **1(BF$_4$)$_2$** (2.111(6)-2.171(3) Å) indicate that they are in the HS state at these temperatures. This suggests that the HS state of **1(BF$_4$)$_2$** is reached at lower temperatures in agreement with the magnetic properties (see below). The coordination geometry is close to the ideal D_{2d} symmetry associated to a $[Fe(bpp)_2]^{2+}$ centre at both temperatures. Thus, trans-N(pyridyl)-Fe-N(pyridyl) angle (ϕ) of 180^{O} and dihedral angle between the least squares planes of the two ligands (θ) of 87^{O} at 120K and 89^{O} at 400 K for **1(ClO$_4$)$_2$** and 88^{O} at 120K and 89^{O} at 350 K for **1(BF$_4$)$_2$** are consistent with those of other bpp complexes exhibiting spin-crossover.[3] The crystal packing of the complexes is very similar at the two temperatures. In both cases, neighboring $[Fe(bppCOOH)_2]^{2+}$ cations are linked through hydrogen bonds between the carboxylic acid groups (dO1···O3 = 2.671 Å at 120 K and dO1···O2 = 2.732 Å at 400 K for **1(ClO$_4$)$_2$** and dO1···O2 = 2.676 Å at 120 K and dO1···O2 = 2.724 Å at 350 K for **1(BF$_4$)$_2$**, Fig. 1), forming a chain that runs along the *b* axis. These chains present numerous short contacts with ClO_4^- or BF_4^- counterions that involve CH groups from pyrazole and pyridine groups. These chains are linked through intermolecular interactions that involve C atoms from a pyrazole group and oxygen atoms from a carboxylic acid group (see Figs. S1, S2 and S3 in the ESI† and associated text). F and O atoms from BF_4^- (**1(BF$_4$)$_2$**) and ClO_4^- (**1(ClO$_4$)$_2$**) are disordered at 350 and 400 K, respectively. This disorder has been solved by considering eight F or O atoms with an occupancy of 50 %. We can conclude then that the presence of the carboxylic acid groups causes a different packing to the "terpyridine embrace" crystal packing motif found in many salts of $[Fe(bpp)_2]^{2+}$ and derivatives, which is a four-fold layer formed by π-π and edge-to-face C-X···π interactions between pyrazole groups of neighboring molecules.[3]

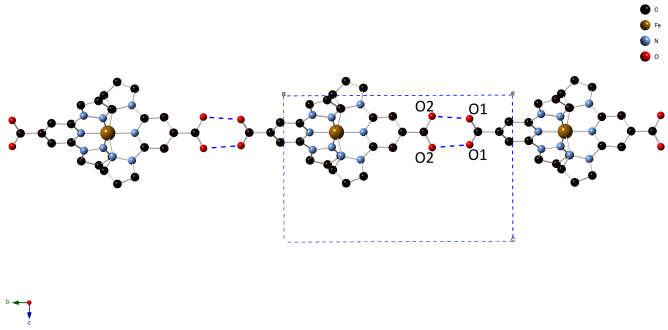

Fig. 1 Chain of hydrogen-bonded $[Fe(bppCOOH)_2]^{2+}$ complexes in the structure of **$1(BF_4)_2$** at 120 K.

The changes in the unit cell with the temperature measured by single crystal X-ray diffraction of the two salts are consistent with an abrupt spin transition (see Figs. S4 and S5 in the ESI†). The most important change is an abrupt expansion of the *b* parameter above 380 K for **$1(ClO_4)_2$** and 340 K for **$1(BF_4)_2$** in the direction of the hydrogen-bonded chains. On the other hand, *a* and *c* parameters and the unit cell volume of **$1(BF_4)_2$** are lower than those of **$1(ClO_4)_2$** in agreement with the bigger size of ClO_4^- counteranion. In contrast to this, the *b* parameters of the two compounds in the LS and HS states are very close. This indicates that the hydrogen-bonded chains of complexes, which run in this direction, are very similar in the two compounds.

Variable-temperature powder X-ray diffraction measurements of **$1(ClO_4)_2$** were performed between 400 and 298 K. The most notable change is the shift to lower 2θ values of the intense diffraction peaks near 2θ = 15 and 18.5° at increasing temperature (see Figs. S6 and S7 in the ESI†). As the position of these peaks changes just below and above the temperature of the spin-transition ($T_{1/2\uparrow}$ = 384 K) (see patterns at 380 and 390 K in Fig. S7 in the ESI†), they correspond to the LS and HS phases. This is confirmed by the pattern measured at an intermediate temperature of 385 K, which shows that the LS and HS peaks coexist in agreement with magnetic properties (see Fig. S7 in the ESI†). PXRD pattern of **$1(BF_4)_2$** at 298 K is consistent with the structure solved at 120 K (see Fig. S8 in the ESI†).

Structure of $[Fe(bppCOOH)_2](CF_3SO_3)_2 \cdot yMe_2CO$ ($1(CF_3SO_3)_2 \cdot yMe_2CO$).

The structure of this compound was solved by single crystal X-ray diffraction at 120 K of a crystal transferred directly to the cold nitrogen stream of the diffractometer from the mother liquor and at 300 K of another crystal, which was previously filtered and stored in air. In both cases, it crystallizes in the orthorhombic system with the centrosymmetric *Pcab* space group. The asymmetric unit is composed by one $[Fe(bppCOOH)_2]^{2+}$ cation, two $CF_3SO_3^-$ anions and one (at 120 K) or half (at 300 K) acetone solvent molecule (see Fig. S9 in the ESI†). Therefore, the compound can be formulated as $[Fe(bppCOOH)_2](CF_3SO_3)_2 \cdot Me_2CO$ at 120 K and $[Fe(bppCOOH)_2](CF_3SO_3)_2 \cdot 0.5Me_2CO$ at 300 K. Fe-N bond lengths lie in the range 1.892(2)-1.968(3) Å at 120 K and 1.897(2)-1.970(3) at 300 K, typical distances of the LS configuration. Neighboring $[Fe(bppCOOH)_2]^{2+}$ cations are linked through hydrogen bonds involving one of the two oxygen atoms from the two carboxylic acid groups (dO1···O4 = 2.673 Å at 120 K and dO1···O4 =2,694 Å at 300 K) forming a zigzag chain that runs along the *b* axis (Fig. 2). The OH group from the carboxylic acids not involved in these hydrogen-bonds forms a hydrogen bond with a triflate counteranion (dO2···O8 = 2.638 Å at 120 K and dO2···O9 =2.654 Å at 300 K) (Fig. 2). These chains are connected through CH··· π interactions, which involve CH groups from pyrazole and pyridine rings, and they present numerous short contacts with surrounding $CF_3SO_3^-$ anions and Me_2CO solvent molecules. Me_2CO molecules do not form hydrogen bonds.

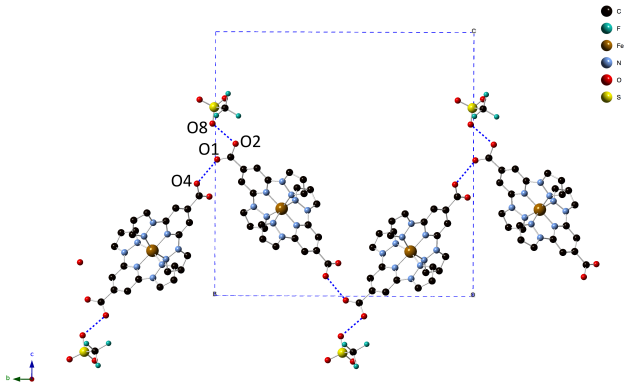

Fig. 2 Hydrogen-bonded $[Fe(bppCOOH)_2]^{2+}$ complexes and triflate anions in the structure of **$1(CF_3SO_3)_2 \cdot yMe_2CO$** at 120 K.

A single crystal of this compound maintains the crystallinity up to 380 K. Above this temperature, the crystal loses it crystallinity and a change of color is observed from red-orange to yellow in good agreement with magnetic properties (see below). Interestingly, it is possible to recover the red-orange color by placing the crystals in an atmosphere saturated in acetone. PXRD pattern at room temperature is consistent with the simulated one obtained from the single crystal X-ray diffraction structure at 300 K (see Fig. S10 in the ESI†). PXRD pattern of the yellow crystals obtained after desolvation change completely with respect to the solvated ones indicating that a new phase is obtained. PXRD pattern of the resolvated sample confirms the recovery of the initial solvated phase (see Fig. S10 in the ESI†). Therefore, the loss of half acetone solvent molecule from 120 to 300 K does not lead to important changes in the structure, while complete removal of acetone solvent molecules at higher temperatures lead to a drastic change in the structure, which is reversible. Thermogravimetric (TG) analysis shows a weight decrease of 2 % below 350 K (see Fig. S11 in the ESI†). This weight loss is lower than the expected one for 0.5 acetone molecules found in the structure of the filtered sample (expected weight loss of

3 %) indicating a higher loss of solvent molecules after extracting the crystals from the mother liquor.

Structure of $[Fe(bppCOOH)_2](AsF_6)_2{\cdot}yMe_2CO$ ($1(AsF_6)_2{\cdot}yMe_2CO$) and $[Fe(bppCOOH)_2](SbF_6)_2{\cdot}yMe_2CO$ ($1(SbF_6)_2{\cdot}yMe_2CO$).

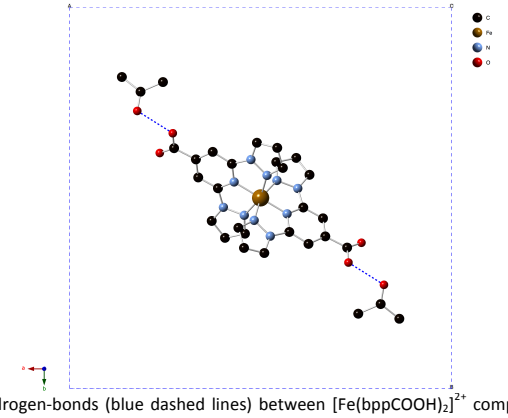

Fig. 3 Hydrogen-bonds (blue dashed lines) between $[Fe(bppCOOH)_2]^{2+}$ complexes and acetone molecules in the structure of **$1(SbF_6)_2{\cdot}yMe_2CO$** at 120 K.

The crystal structures of the two compounds were solved by single crystal X-ray diffraction at 120 K of crystals transferred directly to the cold nitrogen stream of the diffractometer from the mother liquor and at 300 K. They crystallize in the tetragonal system with the non-centrosymmetric $I4_1cd$ space group. The asymmetric unit cell is composed by half $[Fe(bppCOOH)_2]^{2+}$ cation, one AsF_6^- or SbF_6^- anion and one (at 120 K) or half (at 300 K) acetone solvent molecule (see Fig. S12 in the ESI†). Therefore, they can be formulated as $[Fe(bppCOOH)_2](AsF_6)_2{\cdot}2Me_2CO$ or $[Fe(bppCOOH)_2](SbF_6)_2{\cdot}2Me_2CO$ at 120 K and $[Fe(bppCOOH)_2](AsF_6)_2{\cdot}Me_2CO$ or $[Fe(bppCOOH)_2](SbF_6)_2{\cdot}Me_2CO$ at 300 K. The Fe-N bond lengths lie in the range 1.892(4)-1.977(5) Å at 120 K, 1.917(8)-1.997(10) Å at 300 K for **$1(AsF_6)_2{\cdot}yMe_2CO$** and 1.898(4)-1.979(5) Å at 120 K and 1.937(12)-2.023(14) Å at 300 K for **$1(SbF_6)_2{\cdot}yMe_2CO$**. These are typical distances of the LS configuration but the increase of bond lengths with the temperature indicates that there is an increasing fraction of HS molecules with temperature, which is higher for **$1(SbF_6)_2{\cdot}yMe_2CO$,** in agreement with magnetic properties (see below). Neighboring $[Fe(bppCOOH)_2]^{2+}$ cations are not linked through hydrogen bonds as in the previous salts. Thus, their OH groups are involved in hydrogen bonds with carbonyl groups from two neighboring acetone solvent molecules (Figs. 3 and S13 in the ESI†). Neighboring $[Fe(bppCOOH)_2]^{2+}$ in the structures at 120 K present $CH\cdots\pi$ contacts involving the pyrazole rings giving rise to chains that run along the *c* axis surrounded by AsF_6^- or SbF_6^- anions and acetone molecules (see Figs. S12 and S14 in the ESI† and associated text). F atoms from AsF_6^- are disordered at 300 K. This disorder has been solved by considering twelve F atoms with an occupancy of 50 %.

PXRD pattern at room temperature of the two compounds are consistent with the simulated ones obtained from the single crystal X-ray diffraction structure at 300 K (see Fig. S15 in the ESI†). Desolvation by heating at 400 K leads to a color change from red-orange to dark red. PXRD pattern of the desolvated sample changes completely with respect to the solvated ones (see Fig. S15 in the ESI†) indicating that a new phase is obtained. As in **$1(CF_3SO_3)_2{\cdot}yMe_2CO$**, PXRD pattern of the resolvated sample indicates that the initial solvated phase is recovered after contact of the desolvated crystals with acetone vapors (see Figure S15 in the ESI†). TG analysis of freshly prepared samples of **$1(AsF_6)_2{\cdot}yMe_2CO$** and **$1(SbF_6)_2{\cdot}yMe_2CO$** shows a weight decrease of around 6 % in two steps from 300 to 400 K. This decrease is consistent with the expected one for one acetone molecule found in the structure at 300 K (expected weigh loss of 5.7 % for **$1(AsF_6)_2{\cdot}Me_2CO$** and 5.3 % for **$1(SbF_6)_2{\cdot}Me_2CO$**) (see Figure S11 in the ESI†). The temperatures of these weight losses are higher than those of compound **$1(CF_3SO_3)_2{\cdot}yMe_2CO$** in agreement with the lack of hydrogen-bonds of the acetone molecules of this last compound. In contrast to this, elemental analyses of the two compounds in older samples are more consistent with the presence of one acetone and one water molecule. This could suggest absorption of water molecules after filtering the crystals. Elemental analysis of desolvated samples after heating at 400 K for one hour confirms the complete loss of the solvent molecules (see experimental section).

Structure of $[Fe(bppCOOEt)_2](ClO_4)_2{\cdot}yMe_2CO$ ($2(ClO_4)_2{\cdot}yMe_2CO$).

The structure of **$2(ClO_4)_2{\cdot}yMe_2CO$** was solved by single crystal X-ray diffraction at 120 and 300 K. It crystallizes in triclinic crystal system with centrosymmetric *P*-1 space group. This compound can be formulated as $[Fe(bppCOOEt)_2](ClO_4)_2{\cdot}1.5Me_2CO$ at 120 K and $[Fe(bppCOOEt)_2](ClO_4)_2{\cdot}0.75Me_2CO$ at 300 K. Elemental analysis at 300 K is more consistent with two water molecules suggesting a complete loss of acetone solvent molecules and replacement by water molecules after extracting the crystals from the mother liquor or the coexistence of crystals with a different degree of desolvation (see experimental section). The asymmetric unit is composed by two $[Fe(bppCOOEt)_2]^{2+}$ cations, five perchlorate anions (two of them with an occupancy of 0.5 and disorder) and three acetone molecules with an occupancy of 0.5 at 300 K. The iron(II) ions present a distorted octahedral coordination geometry to bppCOOEt ligands similar to that of $[Fe(bppCOOH)_2]^{2+}$ salts (Figs. 4 and S16 in the ESI†). The Fe-N bond lengths at 120 K (1.889(3)-1.975(4) and 1.893(3)-1.974(4) Å) and 300 K (1.889(5)-1.977(6) 1.880(5)-1.987(6) Å) indicate that the complexes are in the LS state in agreement with magnetic measurements. The coordination geometry is close to the ideal D_{2d} symmetry at the two temperatures. Thus, ϕ angles of 177.36(15) and 178.77(15)$^{\circ}$ at 120 K and 178.7(2) and 179.7(2)$^{\circ}$ at 300 K, and θ angles close to 85° at 120 K and 86° K at 300 K, are obtained. These values contrast with those reported for the Fe(II) complex of the methyl ester derivative of bppCOOH (bppCOOMe) (ϕ = 158.77(5)$^{\circ}$ and θ = 80.738(12) $^{\circ}$),[11] which is HS from 2 to 300 K. This confirms that a coordination

geometry close to the ideal D_{2d} symmetry favors LS state and SCO.[3b] The crystal packing of **2(ClO$_4$)$_2$·yMe$_2$CO** at the two temperatures is very different to that of [Fe(bppCOOH)$_2$]$^{2+}$ salts. On one hand, oxygen atoms from the carboxyethylester group of [Fe(bppCOOEt)$_2$]$^{2+}$ complexes cannot form hydrogen bonds. On the other hand, the presence of the bulky ethyl group prevents the formation of the "terpyridine embrace" crystal packing motif. Thus, neighboring [Fe(bppCOOEt)$_2$]$^{2+}$ complexes interact through numerous short contacts involving CH groups of pyrazole and pyridine rings, CO groups or CH_2 and CH_3 groups. This leads to a complicate network of weak intermolecular interactions that include many interactions with perchlorate counterions and acetone solvent molecules. It was not possible to solve the structure at higher temperatures due to the loss of crystallinity after evaporation of solvent molecules. PXRD patterns from 300 to 340 K are consistent with that obtained from the single crystal X-ray diffraction structure at 300 K but, at higher temperatures, a change of phase is observed. The initial solvated phase cannot be recovered after resolvation in contrast to [Fe(bppCOOH)$_2$]$^{2+}$ salts (see Fig. S17 in the ESI†). Elemental analysis of the desolvated sample is consistent with the presence of one water molecule. This could indicate absorption of water from the desolvated sample (see experimental section).

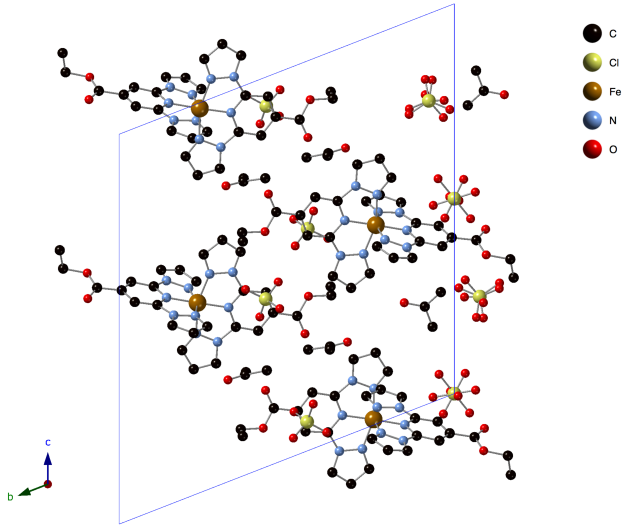

Fig. 4 Projection in the *bc* plane of the structure of **2(ClO$_4$)$_2$·Me$_2$CO** at 120 K.

Magnetic properties.

The temperature dependence of the product of the magnetic susceptibility times temperature (χ_MT) of the [Fe(bppCOOH)$_2$]$^{2+}$ salts is shown in Fig. 5 together with that previously reported for **1(ClO$_4$)$_2$**.[5] χ_MT of **1(ClO$_4$)$_2$** and **1(BF$_4$)$_2$** below 300 K shows a value close to 0, typical of diamagnetic LS state (S=0), in agreement with the crystallographic data at 120 K of the two compounds. At temperatures above 340 K for **1(BF$_4$)$_2$** and 380 K for **1(ClO$_4$)$_2$**, χ_MT shows a sharp increase to values of 3.0 and 3.2 cm^3·K·mol^{-1} at 350 and 390 K, respectively**,** consistent with a LS to HS conversion close to 100 %. In these two compounds the same behavior is observed in heating and cooling modes with a small thermal hysteresis of 3 K ($T_{1/2\uparrow}$ = 349 K and $T_{1/2\downarrow}$ = 345 K for **1(BF$_4$)$_2$** and $T_{1/2\uparrow}$ = 384 K and $T_{1/2\downarrow}$ = 381 K for **1(ClO$_4$)$_2$**). The presence of this thermal hysteresis loop clearly demonstrates the existence of a significant level of cooperativity due to the presence of intermolecular interactions mediated by the hydrogen-bonds between neighboring [Fe(bppCOOH)$_2$]$^{2+}$ complexes. Indeed, **1(AsF$_6$)$_2$·yMe$_2$CO** and **1(SbF$_6$)$_2$·yMe$_2$CO,** the [Fe(bppCOOH)$_2$]$^{2+}$ salts without hydrogen-bonding between the complexes, present a more gradual transition (see below).

Below 350 K, χ_MT of **1(CF$_3$SO$_3$)$_2$·yMe$_2$CO** is consistent to a LS state as suggested by Fe-N bond lengths at 120 and 300 K (see above), with a residual HS probably due to the desolvation of part of the crystals (Fig. 5). Above 350 K, χ_MT shows a sharp increase to a value of 3.5 cm^3·K·mol^{-1} consistent with 100 % of complexes in the HS state. This increase is irreversible as χ_MT is close to 3.5 cm^3·K·mol^{-1} from 400 to 30 K with a decrease below 30 K due to zero-field-splitting as expected for the HS d^6 of Fe(II). This could indicate that the spin transition of this compound is related to the structural changes after losing the solvent molecules in agreement with the change of color and changes observed in single crystal and PXRD measurements and TG measurements (see above).

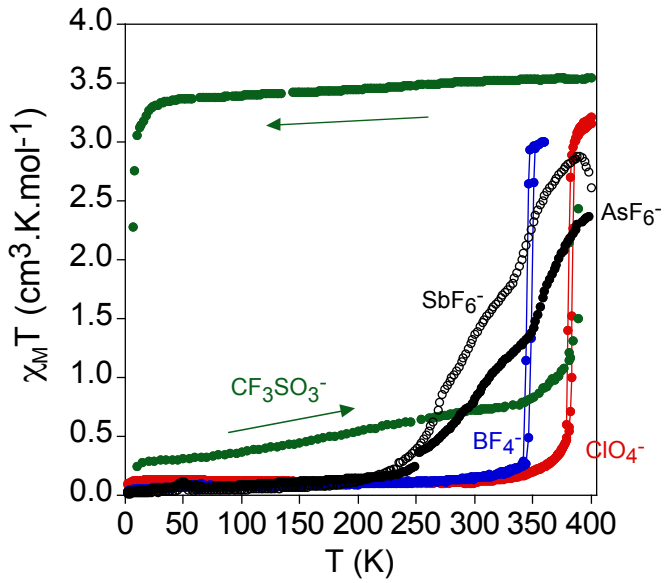

Fig. 5 Thermal dependence of magnetic susceptibility times temperature (χ_MT) of **1(ClO$_4$)$_2$** (red circles), **1(BF$_4$)$_2$** (blue circles), **1(CF$_3$SO$_3$)$_2$·yMe$_2$CO** (green circles), **1(AsF$_6$)$_2$·yMe$_2$CO** (Black circles) and **1(SbF$_6$)$_2$·yMe$_2$CO** (empty circles).

χ_MT of **1(AsF$_6$)$_2$·yMe$_2$CO** and **1(SbF$_6$)$_2$·yMe$_2$CO** shows a value close to 0 cm^3·K·mol^{-1} in the temperature range 2-200 K. At higher temperatures, there is a gradual increase of χ_MT, to reach 2.4 cm^3·K·mol^{-1} at 400 K for **1(AsF$_6$)$_2$·yMe$_2$CO** and 2.9 cm^3·K·mol^{-1} at 390 K for **1(SbF$_6$)$_2$·yMe$_2$CO** indicating a gradual spin transition (Fig. 5). This is consistent with Fe-N bond lengths at 120 and 300 K (see above). The range of temperatures at which the increase of χ_MT is steeper overlaps with those of the weight loss observed in TG analysis (see Fig. S11 in the ESI†). Therefore, it is not possible to determine if they are related to a pure spin transition or desolvation. The presence of steps around 340 K for **1(AsF$_6$)$_2$·yMe$_2$CO** and 330 K

for **1(SbF$_6$)$_2$·yMe$_2$CO** in this first heating could be related to the presence of an intermediate phase by partial loss of acetone solvent molecules as TG analysis of the two compounds shows a step in the weight loss around these temperatures (see Fig. S11 in the ESI†). However, PXRD patterns of **1(AsF$_6$)$_2$·yMe$_2$CO** and **1(SbF$_6$)$_2$·yMe$_2$CO** only show a clear and irreversible change of phase at temperatures close to 400 K (see Fig. S15 in the ESI†). Furthermore, single crystal unit cell measurements at temperatures above from 300 to 400 K show a progressive decrease of unit cell volume and loss of crystallinity with time but they do not show a drastic change in the unit cell. In these two compounds, the complete loss of acetone molecules at higher temperatures leads to a decrease of χ_MT above 390 K to reach 1.8 cm^3·K·mol^{-1} for **1(AsF$_6$)$_2$·yMe$_2$CO** and 2.5 cm^3·K·mol^{-1} for **1(SbF$_6$)$_2$·yMe$_2$CO** at 400 K. χ_MT of the desolvated compounds, obtained in the cooling mode after heating to 400 K, decreases gradually to reach values below 0.3 cm^3·K·mol^{-1} from 200 to 2 K (see Fig. S18 in the ESI†) with a $T_{1/2}$ of 400 K for **1(AsF$_6$)$_2$** and 365 K for **1(SbF$_6$)$_2$**. Desolvation in the two compounds decreases the HS fraction above 250 K but does not cause drastic changes in the magnetic behavior. Thus, gradual spin transitions are still observed in the desolvated phases with a higher HS fraction for **1(SbF$_6$)$_2$** than that of **1(AsF$_6$)$_2$**.

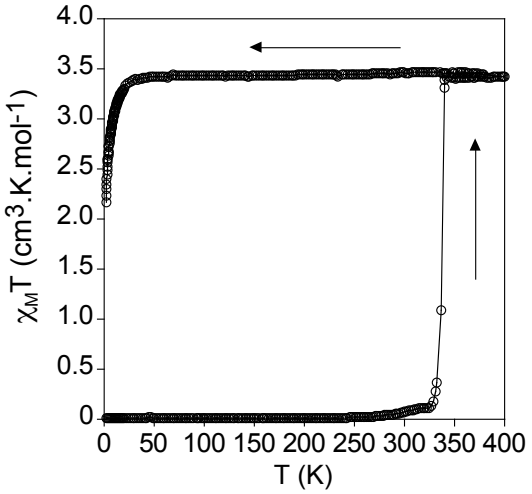

Fig. 6 Thermal dependence of magnetic susceptibility times temperature (χ_MT) of **2(ClO$_4$)$_2$·yMe$_2$CO**.

χ_MT of **2(ClO$_4$)$_2$·yMe$_2$CO** is close to 0 below 300 K in agreement with Fe-N bond lengths at 120 and 300 K. Above 330 K, χ_MT shows a sharp increase to a value of 3.5 cm^3·K·mol^{-1} consistent with 100 % of complexes in the HS state. This increase is irreversible as χ_MT measured from 400 to 2 K remain almost constant and close to this value with a decrease below 30 K due to zero-field-splitting as expected for the HS d^6 of Fe(II) (Fig. 6). This indicates again that the spin transition is related here with structural changes after losing the solvent molecules. Indeed, powder PXRD measurements support this hypothesis as they show an irreversible change of phase due to desolvation (see above).

The decrease in the $T_{1/2}$ with decreasing counteranion size of **1(BF$_4$)$_2$** with respect to that of **1(ClO$_4$)$_2$** contrasts to that observed for **1(AsF$_6$)$_2$·yMe$_2$CO** and **1(SbF$_6$)$_2$·yMe$_2$CO**. Thus, in these two compounds, the opposite trend is observed and the bulkier counteranion stabilizes the HS state and gives rise to a lower $T_{1/2}$ in **1(SbF$_6$)$_2$·yMe$_2$CO**. These two trends have been observed for BF_4^- and ClO_4^- salts of iron(II) complexes of similar ligands. Thus, whereas ClO_4^- stabilizes the HS state in isostructural salts of $[Fe(bpp)_2]^{2+}$ with variable BF_4^- and ClO_4^- contents,[12] or iron(II) complexes of 4-methyl-2,6-di(pyrazol-1-yl)-pyridine,[13] 4-(isopropylsulfan-yl)-2,6-di(pyrazol-1-yl)pyridine)[14] and 1,10-phenanthroline-2-carbaldehydephenylhydrazone),[15] there are examples of the opposite behavior.[16,17] It was concluded that there is no predictable relationship between anion size and $T_{1/2}$, even between salts that are known to be crystallographically isostructural.[15] A possible explanation of this opposite trend in our compounds is that in **1(BF$_4$)$_2$** and **1(ClO$_4$)$_2$**, the packing of the complexes is dominated by the hydrogen-bonding along the *b* axis resulting in very similar unit cell parameters and chemical pressure in the two compounds. Due to this, the counteranion size does not affect the chemical pressure of the complexes and other factors such as the electronegativity of the counteranions become more important. Indeed, there are many short contacts among the $[Fe(bppCOOH)_2]^{2+}$ complexes and counteranions which could result in a different withdrawal of electron density and changes in the crystal field around iron(II). In **1(AsF$_6$)$_2$·yMe$_2$CO** and **1(SbF$_6$)$_2$·yMe$_2$CO**, which do not present this type of packing and show smaller differences in the electronegativity, the changes in unit cell volume and chemical pressure induced by the size of the counteranion become the decisive parameter.

Photomagnetic properties.

1(ClO$_4$)$_2$, **1(BF$_4$)$_2$**, **1(CF$_3$SO$_3$)$_2$·yMe$_2$CO**, **1(AsF$_6$)$_2$·yMe$_2$CO**, **1(SbF$_6$)$_2$·yMe$_2$CO** and **2(ClO$_4$)$_2$·yMe$_2$CO**, have been irradiated at 10 K at 532, 650, 830 or 980 nm. A drastic increase of the magnetic signal was observed after irradiation at 532 nm for all the compounds. After the irradiation was switched off, the temperature was increased at 0.3 K·min^{-1} and the magnetic susceptibility recorded (so called *T*(LIESST) experiment) (see Fig. 7). The fraction of Fe(II) photoconverted after irradiation is calculated to be around 30 % for **1(AsF$_6$)$_2$·yMe$_2$CO** and 40 % for **2(ClO$_4$)$_2$·yMe$_2$CO**. The other compounds showed an almost quantitative LS to HS photoconversion (70 % or higher). The *T*(LIESST), defined as the minimum of the derivative of χ_MT with temperature, is 41 K for **1(CF$_3$SO$_3$)$_2$·yMe$_2$CO**, 54 K for **1(AsF$_6$)$_2$·yMe$_2$CO**, 57 K for **1(SbF$_6$)$_2$·yMe$_2$CO,** 60 K for **1(ClO$_4$)$_2$**, 67 K for **1(BF$_4$)$_2$** and 71 K for **2(ClO$_4$)$_2$·Me$_2$CO**. The *T*(LIESST) curves of the $[Fe(bppCOOH)_2]^{2+}$ compounds with hydrogen-bonds (**1(BF$_4$)$_2$**, **1(ClO$_4$)$_2$** and **1(CF$_3$SO$_3$)$_2$·yMe$_2$CO**) show abrupt LIESST relaxation curves. In contrast to this, 1**(AsF$_6$)$_2$·yMe$_2$CO** and **1(SbF$_6$)$_2$·yMe$_2$CO**, which present weaker intermolecular interactions, show more gradual LIESST curves (Fig. 7). The *T*(LIESST) values for these compounds may be compared with

those previously obtained for other bpp compounds. For this family of compounds, it has been proposed a linear correlation between the thermal spin crossover and the *T*(LIESST).[18] These two physical quantities may be related by the formula *T*(LIESST) = $T_0 - 0.3T_{1/2}$, with T_0 = 150 K. Taking 383 and 347 K as the mean values of $T_{1/2}$ of **1(ClO$_4$)$_2$** and **1(BF$_4$)$_2$**, respectively, *T* (LIESST) of 35.1 and 45.9 K are expected for these two compounds (ca. 20 K below the observed ones of 60 and 67 K). The same effect was observed for [Fe(bpp-triolH$_3$)$_2$](ClO$_4$)$_2$, where bpp-triolH$_3$ is an amide derived from bppCOOEt with triolH$_3$ = C(O)NHC(CH$_2$OH)$_3$.[9] In the other compounds of this work, it is not possible to know the $T_{1/2}$ as the change of spin state with the temperature is related to desolvation. Thus, the "real $T_{1/2}$" is hidden by the desolvation of the compounds. From these results, it seems that the empirical formula used for bpp presents an important deviation for bppCOOH and related ligands. This could indicate that they present a higher T_0 (close to 170 K) or that *T*(LIESST) of compounds with high $T_{1/2}$ deviates significantly from that formula as observed for other Fe(II) with tridentate ligands.[19] Very recently, it has been proposed that a complicated relationship between *T*(LIESST) and $T_{1/2}$ may reflect low-temperature thermal and light-induced symmetry breaking.[14]

In order to get some insights into the decay of the photo-excited state, kinetics of relaxation of **1(ClO$_4$)$_2$** were recorded for different temperatures (see Fig. S19 in the ESI† and associated text). The decay of the photoinduced HS state of this compound is faster at high temperatures, consistent with a thermally activated process. It can also be observed that the decay is not exponential. The kinetics has been fitted using a so-called sigmoidal law. This law describes a self-accelerated process, often associated with cooperative systems. This cooperativity arises from the large difference in metal-ligand bond lengths, resulting in elastic interactions caused by change in internal pressure as the spin transition proceeds.[20] In a recent article, Paulsen and coworkers have been able to derive cooperativity parameter using DFT ab initio calculations. Thanks to these calculations, the degree of cooperativity in two solvatomorphs, Fe(pic)$_3$Cl$_2$·EtOH (abrupt transition) and Fe(pic)$_3$Cl$_2$·MeOH (gradual transition), was recovered. Cooperativity and degree of octahedricity of Fe centers have been linked, emphasizing that difference in metal-ligand bond lengths is not the only factor governing cooperativity.

Magnetization under irradiation of **1(ClO$_4$)$_2$** as a function of the temperature has been recorded. More precisely, the temperature was decreased continuously from 100 K to 10 K under continuous irradiation (532 nm). The temperature was then re-increased up to 100 K, still under irradiation (see Figs. S20 and S21 in the ESI† and associated text). A clear light-induced thermal hysteresis (LITH)[22] is observed below 70 K. This compound seems then to be cooperative enough to present a static LITH.

Conclusions

In this work, we have prepared and characterized five salts of [Fe(bppCOOH)$_2$]$^{2+}$. They present a variety of magnetic behaviors with reversible temperature-, light- and solvent-induced spin transitions, which is difficult to rationalize as it corresponds to compounds with different structures and, therefore, different crystal packings and intermolecular interactions. This dependence of the magnetic properties on the counteranion and solvent molecule is not unusual and has been found in other bpp and 3-bpp derivatives (3-bpp = 2,6-bis(pyrazol-3-yl)pyridine).[12-17,23-25] Some general conclusions, however, can be extracted.

For small tetrahedral counteranions such as ClO_4^- or BF_4^-, the isostructural compounds **1(ClO$_4$)$_2$** and **1(BF$_4$)$_2$** were obtained. In these compounds, the absence of solvate molecules and the presence of a hydrogen-bonded chain of complexes lead to abrupt and reversible SCO. Furthermore, the decrease of size of the counteranion favors the HS state leading to a lower $T_{1/2}$ for **1(BF$_4$)$_2$**. This decrease of $T_{1/2}$ of ca 40 K could be related to the greater withdrawal of electronic density for the BF_4^- counteranion. The use of counteranions of larger size leads to the incorporation of solvent molecules in the structure in compounds **1(CF$_3$SO$_3$)$_2$·yMe$_2$CO, 1(AsF$_6$)$_2$·yMe$_2$CO** and **1(SbF$_6$)$_2$·yMe$_2$CO**, which play an important role in their magnetic properties. Thus, the loss of solvent molecules in these complexes is accompanied with irreversible spin transitions of different sign. Thus, whereas desolvated **1(CF$_3$SO$_3$)$_2$·yMe$_2$CO** is 100 % HS, desolvation of **1(AsF$_6$)$_2$·yMe$_2$CO** and **1(SbF$_6$)$_2$·yMe$_2$CO** do not induce important changes in the spin state of the [Fe(bppCOOH)$_2$]$^{2+}$ complexes. Interestingly, these changes are reversible as resolvated samples recover the structure and color of the initial samples. Therefore, **1(CF$_3$SO$_3$)$_2$·yMe$_2$CO** presents a reversible solvent-induced spin transition. The increase of size of SbF_6^- with respect to AsF_6^- in the isostructural **1(AsF$_6$)$_2$·yMe$_2$CO** and **1(SbF$_6$)$_2$·yMe$_2$CO** salts, lead to a stabilization of the HS state and to a lower $T_{1/2}$ in contrast to ClO_4^- and BF_4^- salts. This trend could suggest that, in the absence of the hydrogen-bonded chain of complexes found in **1(ClO$_4$)$_2$** and **1(BF$_4$)$_2$**, the expansion of unit cell volume by the larger SbF_6^- counterion becomes the most important factor.

The use of the ethyl ester derivative bppCOOEt in the place of bppCOOH has a similar effect to that of the use of the bulkier counteranions. Thus, an irreversible spin transition is obtained in **2(ClO$_4$)$_2$·yMe$_2$CO** as a result of the loss of solvent molecules after heating above 340 K. However, in contrast to the [Fe(bppCOOH)$_2$]$^{2+}$ salts, the original structure is not recovered after resolvation. This could indicate that the carboxylic acid group could play a role in the reversibility of the solvation or that the flexibility of the ethyl group favor the formation of different structures for the solvated and resolvated compound.

All these results indicate that the spin state of [Fe(bppCOOH)$_2$]$^{2+}$ complex is very sensitive to the counteranion and solvent molecules and that the LS state is not as favored as the first results obtained with the ClO_4^- salt could suggest. All these compounds show a clear LIESST effect. As expected, the lower $T_{1/2}$ of the BF_4^- salt, gives rise to an increase of the *T*(LIESST) with respect to that of **1(ClO$_4$)$_2$**.[5] Finally, an interesting point of **1(AsF$_6$)$_2$·yMe$_2$CO** and

1(SbF$_6$)$_2$·yMe$_2$CO is that they crystallize in a non-centrosymmetric space group. This could open the way to other phenomena in coexistence with the thermal-, photo- and solvent-induced SCO of these compounds such as ferroelectricity, which has been recently reported for a salt of $[Fe(3\text{-bpp})_2]^{2+}$.[26]

Experimental

General Remarks. 2,6-di(1H-pyrazol-1-yl)isonicotinic acid (bppCOOH), bppCOOEt and $[Fe(bppCOOH)_2](ClO_4)_2$ (**1(ClO$_4$)$_2$**) were prepared according to the literature methods.[5,10,27] All other chemicals are commercially available and were used as received without further purification. Syntheses of **1(BF$_4$)$_2$**, **1(CF$_3$SO$_3$)$_2$·yMe$_2$CO**, **1(AsF$_6$)$_2$·yMe$_2$CO** and **1(SbF$_6$)$_2$·yMe$_2$CO** were carried out in deoxygenated solvents under inert atmosphere of N_2 using glovebox techniques. All other materials and solvents were commercially available and used without further purification.

Synthesis of [Fe(bppCOOH)$_2$](BF$_4$)$_2$ (1(BF$_4$)$_2$). $Fe(BF_4)_2{\cdot}6H_2O$ (17.5 mg, 0.05 mmol) was added to a solution of bppCOOH (28,5 mg, 0.10 mmol) in acetone (3 mL) and the mixture was stirred for 15 minutes. An orange solution was formed. Red prismatic crystals of $[Fe(bppCOOH)_2](BF_4)_2$ suitable for X-ray diffraction were obtained by slow diffusion of diethyl ether into this solution. $FeC_{24}H_{18}N_{10}O_4B_2F_8$ (739.95): calcd. C 38.96, N 18.93, H 2.45; found C 38.31, N 18.54, H 2.60.

Synthesis of [Fe(bppCOOH)$_2$](CF$_3$SO$_3$)$_2$·yMe$_2$CO (1(CF$_3$SO$_3$)$_2$·yMe$_2$CO). A solution of $Fe(CF_3SO_3)_2$ (35.4 mg, 0.10 mmol) in acetone (2 mL) was added to a solution of bppCOOH (57 mg, 0.20 mmol) in acetone (10 mL) and the mixture was stirred for 15 minutes. A solution was formed. Red prismatic crystals of $[[Fe(bppCOOH)_2](CF_3SO_3)_2{\cdot}yMe_2CO$ suitable for X-ray diffraction were obtained by slow diffusion of diethyl ether into this solution. $FeC_{27}H_{24}N_{10}O_5Sb_2F_{12}$ (1095.93): calcd. for **1(CF$_3$SO$_3$)$_2$·Me$_2$CO** C 37.76, N 15.18, H 2.62, S 6.95; found C 37.76, N 15.26, H 2.35, S 6.65.

Synthesis of [Fe(bppCOOH)$_2$](AsF$_6$)$_2$·yMe$_2$CO (1(AsF$_6$)$_2$·yMe$_2$CO). $FeCl_2$ (3.2 mg, 0.025 mmol) was added to a solution of $AgAsF_6$ (14.8 mg, 0.05 mmol) in acetone (1.5 mL). The AgCl precipitate was filtered. Then the solution was added to another solution of bppCOOH (14.2 mg, 0.05 mmol) in acetone (1.5 mL) and the mixture was stirred for 15 minutes. An orange solution was formed. Orange needle-like crystals of $[Fe(bppCOOH)_2](AsF_6)_2{\cdot}yMe_2CO$ suitable for X-ray diffraction were obtained by slow diffusion of diethyl ether into this solution. $FeC_{27}H_{26}N_{10}O_6As_2F_{12}$ (1020.29): calcd. for **1(AsF$_6$)$_2$·Me$_2$CO·H$_2$O** C 31.79, N 13.73, H 2.57; found C 31.82, N 13.57, H 2.71. $FeC_{24}H_{18}N_{10}O_4As_2F_{12}$ (944.13): calcd. for **1(AsF$_6$)$_2$** C 30.53, N 14.84, H 1.92; found C 30.39, N 14.76, H 1.91 (desolvated sample).

Synthesis of [Fe(bppCOOH)$_2$](SbF$_6$)$_2$·yMe$_2$CO (1(SbF$_6$)$_2$·yMe$_2$CO). $FeCl_2$ (15.8 mg, 0.125 mmol) was added to a solution of $AgSbF_6$ (85.9 mg, 0.25 mmol) in acetone (2.5 mL). The AgCl precipitate was filtered. Then the solution was added to another solution of bppCOOH (72 mg, 0.25 mmol) in acetone (12.5 mL) and the mixture was stirred for 15 minutes. An orange solution was formed. Orange needle-like crystals of $[Fe(bppCOOH)_2](SbF_6)_2{\cdot}yMe_2CO$ suitable for X-ray diffraction were obtained by slow diffusion of diethyl ether into this solution. $FeC_{27}H_{26}N_{10}O_6Sb_2F_{12}$ (1113.91): calcd. for **1(SbF$_6$)$_2$·Me$_2$CO·H$_2$O** C 29.11, N 12.57, H 2.35; found C 29.80, N 12.29, H 2.46. $FeC_{24}H_{18}N_{10}O_4Sb_2F_{12}$ (1037.81): calcd. for **1(SbF$_6$)$_2$** C 27.78, N 13.50, H 1.75; found C 27.46, N 13.43, H 1.72 (desolvated sample).

Synthesis of [Fe(bppCOOEt)$_2$](ClO$_4$)$_2$·yMe$_2$CO (2(ClO$_4$)$_2$·yMe$_2$CO). A solution of $Fe(ClO_4)_2.xH_2O$ (12.5 mg, 0.05 mmol) in acetone (3 mL) was added to a solution of bppCOOEt (28 mg, 0.10 mmol) in acetone (3 mL) and the mixture was stirred for 15 minutes. Red prismatic crystals of **2(ClO$_4$)$_2$·Me$_2$CO** suitable for X-ray diffraction were obtained by slow diffusion of diethyl ether into this solution. Calcd. for **2(ClO$_4$)$_2$·2H$_2$O** C 39.23, N 16.34, H 3.53; found C 38.87, N 16.06, H 3.33. Calcd. for **2(ClO$_4$)$_2$·H$_2$O** C 40.07, N 16.69, H 3.36; found C 39.70, N 16.56, H 3.20 (desolvated sample).

Structural characterization. Single crystals of all the complexes were mounted on a glass fiber using a viscous hydrocarbon oil to coat the crystal and then transferred directly to the cold nitrogen stream for data collection. X-ray data were collected at 120 K for all compounds, 400 K for **1(ClO$_4$)$_2$**, 350 K for **1(BF$_4$)$_2$** and 300 K for **1(CF$_3$SO$_3$)$_2$·yMe$_2$CO**, **1(AsF$_6$)$_2$·yMe$_2$CO**, **1(SbF$_6$)$_2$·yMe$_2$CO** and **2(ClO$_4$)$_2$·yMe$_2$CO** on a Supernova diffractometer equipped with a graphite-monochromated Enhance (Mo) X-ray Source (λ = 0.71073 Å). The program CrysAlisPro, Oxford Diffraction Ltd., was used for unit cell determinations and data reduction. Empirical absorption correction was performed using spherical harmonics, implemented in the SCALE3 ABSPACK scaling algorithm. Crystal structure was solved by direct methods with the SIR97 program,[28] and refined against all F^2 values with the SHELXL-2013 program,[29] using the WinGX graphical user interface.[30] The structure of **2(ClO$_4$)$_2$·yMe$_2$CO** was solved with the ShelXT structure solution program[31] and refined with the SHELXL-2013 program,[29] using Olex2.[32] Non-hydrogen atoms were refined anisotropically, and hydrogen atoms were placed in calculated positions refined using idealized geometries (riding model) and assigned fixed isotropic displacement parameters. Crystallographic data are summarized in Table S2 in the ESI†. CCDC-1856804-1856814 contain the supplementary crystallographic data for this paper. These data can be obtained free of charge from The Cambridge Crystallographic Data Centre via www.ccdc.cam.ac.uk/data_request/cif. For X-Ray powder pattern, a 0.5 mm glass capillary was filled with a polycrystalline sample of de complexes and mounted and aligned on an Empyrean PANalytical powder diffractometer, using CuKα radiation (λ = 1.54177 Å). A total of 2 scans were collected at room temperature in the 2θ range 5-40º.

Physical characterization. The elemental ratios were measured on a Philips ESEM X230 scanning electron microscope equipped with an EDAX DX-4 microsonde. TG analysis was carried out using a Mettler Toledo TGA/SDTA 851 apparatus. Magnetic measurements were performed with a Quantum Design MPMS-XL-5 SQUID magnetometer in the 2 to 400 K temperature range with an applied magnetic field of 0.1

T at a scan rate of 2 K/min (1 K/min for **1(BF$_4$)$_2$**) on a polycrystalline sample. Irradiation at 532, 650, 830 and 980 nm was produced by laser diodes. The photomagnetic sample consisted of a thin layer of compound whose weight was obtained by comparison of the thermal spin crossover curve with that of a more accurately weighted sample of the same material. Our previously published standardized method for obtaining LIESST was followed.[18] After slowly cooling to 10 K, the sample was irradiated and the change of magnetism followed. When the saturation point was reached, the laser was switched off and the temperature increase at a rate of 0.3 K min^{-1}. The magnetization was measured every 1 K.

Conflicts of interest

There are no conflicts to declare.

Acknowledgements

Financial support from the EU (ERC Advanced Grant Mol-2D and COST Action CA15128 Molecular Spintronics (MOLSPIN)), the Spanish MINECO (MAT2017-89993-R and Unidad de Excelencia María de Maeztu MDM-2015-0538), the Generalitat Valenciana (Prometeo) is gratefully acknowledged. We thank J. M. Martínez-Agudo and G. Agustí from the Universidad de Valencia for the magnetic measurements.

Notes and references

1 See for general reviews: Eds. P. Gütlich and H.A. Goodwin, Spin Crossover in Transition Metal Compounds, *Topics in Current Chemistry*, Springer Verlag, Berlin-Heidelberg-New York, 2004, vols. *233-235*. Ed. M. A. Halcrow, Spin-Crossover Materials: Properties and Applications, John Wiley & Sons, Chichester, UK, 2013.

2 K. S. Kumar and M. Ruben, *Coord. Chem. Rev.*, 2017, **346**, 176.

3 (a) M. A. Halcrow, *Coord. Chem. Rev.,* 2005, **249**, 2880; (b) M. A. Halcrow, *Coord. Chem. Rev.*, 2009, **253**, 2493; (c) J. Olguín and S. Brooker, *Coord. Chem. Rev.*, 2011, **255**, 203; (d) M. A. Halcrow, *New J. Chem.*, 2014, **38**, 1868; (e) L. J. Kershaw Cook, R. Mohammed, G. Sherborne, T. D. Roberts, S. Alvarez and M. A. Halcrow, *Coord. Chem. Rev.,* 2015, **289–290**, 2–12.

4 G. Chastanet, C. A. Tovee, G. Hyett, M. A. Halcrow and J. F. Létard, *Dalton Trans.,* 2012, **41**, 4896.

5 A. Abhervé, M. Clemente-León, E. Coronado, C. J. Gómez-Garcia and M. López-Jordà, Dalton Trans., 2014, **43**, 9406.

6 A. Abhervé, M. J. Recio-Carretero, M. López-Jordà, J. M. Clemente-Juan, J. Canet-Ferrer, A. Cantarero, M. Clemente-León and E. Coronado, *Inorg. Chem.,* 2016, **55**, 9361.

7 V. García-López, A. Abhervé, C. Legendre, I. Pellicer-Carreño, M. Palacios-Corella, A. López-Muñoz, S. Tatay, M. Clemente-León, E. Coronado, E. Pellegrin, J. Herrero-Martín, P. Sainctavit, E. Otero, Manuscript in preparation.

8 V. García-López, F.J. Orts-Mula, M. Palacios-Corella, J.M. Clemente-Juan, M. Clemente-León and E. Coronado, *Polyhedron*, 2018, **150**, 54.

9 L. Rigamonti, N. Bridonneau, G. Poneti, L.Tesi, L. Sorace, D. Pinkowicz, J. Jover, E. Ruiz, R. Sessoli and A. Cornia, *Chem. Eur. J.*, 2018, **24**, 8857.

10 T. Vermonden, D. Branowska, A. T. M. Marcelis and E. J. R. Sudhölter, *Tetrahedron*, 2003, **59**, 5039.

11 N. Bridonneau, L. Rigamonti, G. Poneti, D. Pinkowicz, A. Forni and A. Cornia, *Dalton Trans.*, 2017, **46**, 4075.

12 C. Carbonera, C. A. Kilner, J. F. Létard and M. A. Halcrow, *Dalton Trans.*, 2007, 1284.

13 L. J. Kershaw Cook, F. L. Thorp-Greenwood, T. P. Comyn, O. Cespedes, G. Chastanet and M. A. Halcrow, *Inorg. Chem.*, 2015, **54**, 6319.

14 R. Kulmaczewski, E. Trzop, L. J. Kershaw Cook, E. Collet, G. Chastanet and M. A. Halcrow, *Chem. Commun.*, 2017, **53**, 13268.

15 E. König, G. Ritter, A. K. Kulshreshtha, J. Waigel and H. A. Goodwin, *Inorg. Chem.*, 1984, **23**, 1896.

16 C. Carbonera, J. S. Costa, V. A. Money, J. Elhaïk, J. A. K. Howard, M. A. Halcrow and J. F. Létard, *Dalton Trans.*, 2006, 3058.

17 M. A. Halcrow, *Chem. Soc. Rev.*, 2011, **40**, 4119.

18 (a) T. Buchen, P. Gutlich, K. H. Sugiyarto and H. A. Goodwin, *Chem. Eur. J.*, 1996, **2**, 1134; (b) J.-F. Létard, P. Guionneau, L. Rabardel, J. A. K. Howard, A. E. Goeta, D. Chasseau and O. Kahn, *Inorg. Chem.*, 1998, **37**, 4432; (c) J.-F. Létard, L. Capes, G. Chastanet, N. Moliner, S. Létard, J. A. Real and O. Kahn, *Chem. Phys. Lett.*, 1999, **313**, 115; (d) S. Marcen, L. Lecren, L. Capes, H. A. Goodwin and J.-F. Létard, *Chem. Phys. Lett.*, 2002, **358**, 87; (e) J.-F. Létard, P. Guionneau, O. Nguyen, J. S. Costa, S. Marcen, G. Chastanet, M. Marchivie and L. Capes, *Chem. Eur. J.*, 2005,**11**, 4582; (f) J.-F. Létard, *J. Mater. Chem.*, 2006, **16**, 2550.

19 C. Sánchez-Sánchez, C. Desplanches, J. M. Clemente-Juan, M. Clemente-León and E. Coronado, *Dalton Trans.,* 2017, **46**, 2680.

20 (a) A. Hauser, P. Gütlich and H. Spiering, *Inorg. Chem.,* 1986, **25**, 4245; (b) A. Hauser, *Top. Curr. Chem.*, 2004, **234**, 155.

21 S. Vela and H. Paulsen, *Inorg. Chem.,* 2018, **57,** 9478.

22 F. Varret, K. Boukheddaden, E. Codjovi, C. Enachescu and J. Linarès, *Top. Curr. Chem.*, 2004, **234**, 199.

23 (a) K.H. Sugiyarto and H.A. Goodwin, *Aust. J. Chem.,* 1988, **41** 1645; (b) K. H. Sugiyarto, D. C. Graig, A. D. Rae and H. A. Goodwin, *Aust. J. Chem.,* 1994, **47**, 869; (c) K. H. Sugiyarto, K. Weitzner, D. C. Graig and H. A. Goodwin, *Aust. J. Chem.,* 1997, **50**, 869; (d) K. H. Sugiyarto, M. L. Scudder, D. C. Graig and H. A. Goodwin, *Aust. J. Chem.,* 2000, **53**, 755.

24 (a) M. Nihei, L. Han and Hiroki Oshio, *J. Am. Chem. Soc.*, 2007, **129**, 5312; (b) M. Nihei, H. Tahira, N. Takahashi, Y. Otake, Y. Yamamura, K. Sait, and H. Oshio, *J. Am. Chem. Soc.,* 2010, **132**, 3553.

25 (a) G. A. Graig, J. S. Costa, O. Roubeau, S. J. Teat and G. Aromí, *Chem. Eur. J.,* 2011, **17**, 3120; (b) G. A. Graig, J. S. Costa, O. Roubeau, S. J. Teat and G. Aromí, *Chem. Eur. J.,* 2012, **18**, 11703; (c) G. A. Graig, O. Roubeau and G. Aromí, Coord. *Chem. Rev.*, 2014, **269**, 13.

26 V. Jornet-Mollá, Y. Duan, C. Giménez-Saiz, Y. Y. Tang, P. F. Li, F. M. Romero and R. G. Xiong, *Angew. Chem. Int. Ed.*, 2017, **56**,14052.

27 R. A. Fallahpour, *Synthesis*, 2000, **8**, 1138.

28 A. Altomare, M. C. Burla, M. Camalli, G. L. Cascarano, C. Giacovazzo, A. Guagliardi, A. G. G. Moliterni, G. Polidori and R. Spagna, *J. Appl. Cryst.*, 1999, **32**, 115.

29 G. M. Sheldrick, *Acta Cryst.*, 2015, **C71,** 3.

30 L. J. Farrugia, *J. Appl. Cryst.*, 2012, **45**, 849.

31 G. M. Sheldrick, *Acta Cryst.,* 2015, **A71,** 3.

32 O. V. Dolomanov, L. J. Bourhis, R. J. Gildea, J. A. K. Howard, H. Puschmann, *J. Appl. Cryst.* 2009, **42**, 339.

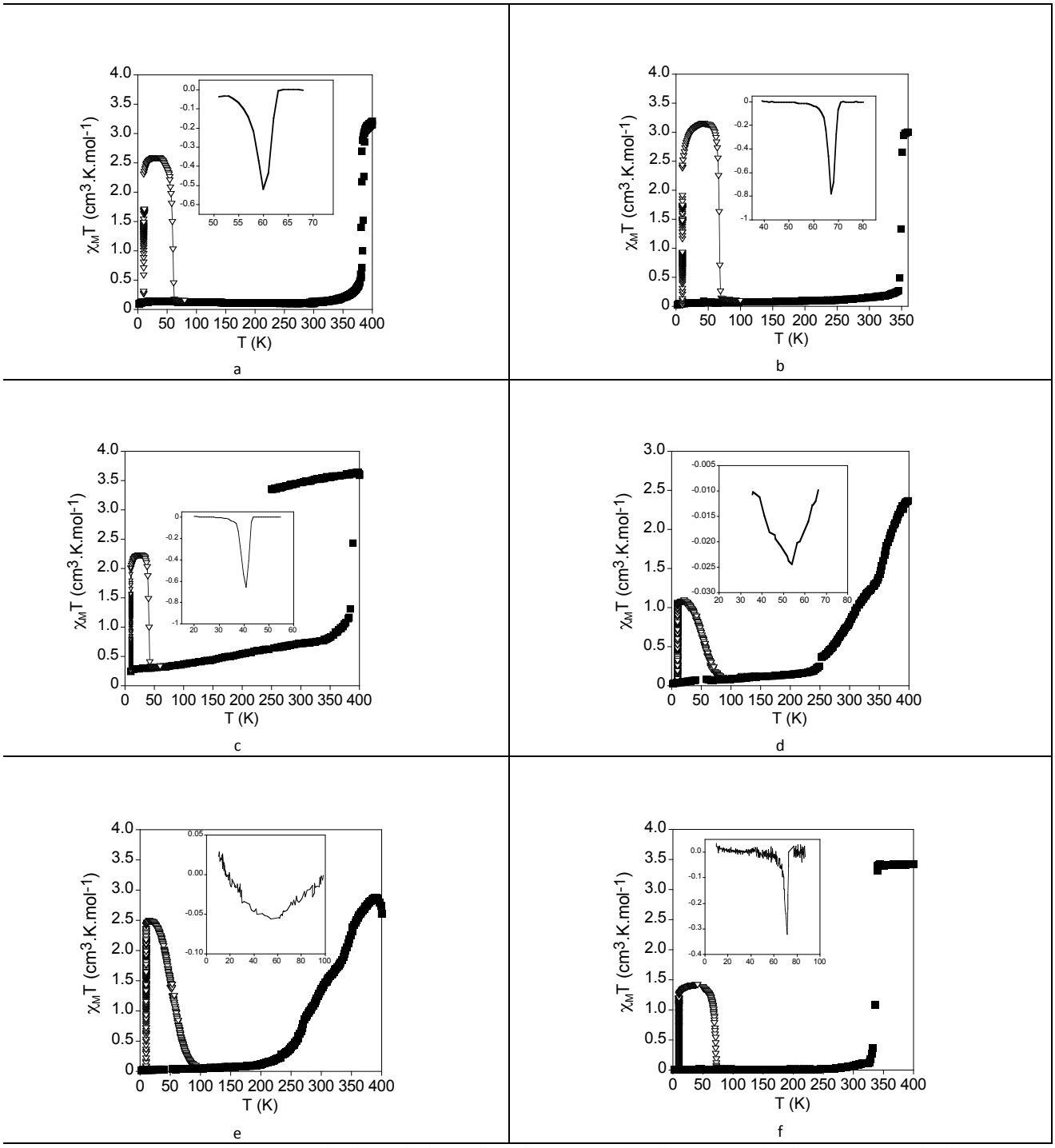

Fig. 7 Thermal variation of $\chi_M T$ for of **1(ClO$_4$)$_2$** (a), **1(BF$_4$)$_2$** (b), **1(CF$_3$SO$_3$)$_2$·yMe$_2$CO** (c), **1(AsF$_6$)$_2$·yMe$_2$CO** (d), **1(SbF$_6$)$_2$·yMe$_2$CO** (e) and **2(ClO$_4$)$_2$·Me$_2$CO** (f). Full squares: data recorded without irradiation; empty triangles: data recorded after irradiation at 10 K. The inset graph shows the temperature dependence of the first derivative of $\chi_M T$ with respect to the temperatur

Journal Name

ARTICLE